Stability augmentation of helicopter rotor blades using passive damping of shape memory alloys

Chul Yong Yun*, Dae Sung Kim and Seung Jo Kim*****
School of Mechanical and Aerospace Engineering,
Seoul National University, Korea 151-742

Abstract

In this study, shape memory alloy damper with characteristics of pseudoelastic hysteresis for helicopter rotor blades are investigated. SMAs can be available in damping augmentation of vibrating structures. SMAs show large hysteresis in the process of pseudoelastic austenite-martensite phase transformation which takes place while subjected to loading above the austenite finish temperature. Since SMAs display pseudoelastic hysteresis behavior over large strain ranges, a significant amount of energy dissipation is possible. A damper can be designed with SMA wires prestressed to a baseline level somewhere in the middle of the pseudoelastic stress range. An experimental study of the effects of pre-strain and cyclic strain amplitude as well as frequency on the damping behavior of pseudoelastic shape memory alloy wires are performed. The effects of the shape memory alloy damper on aeroelastic and ground resonance stability of helicopter are studied. In aeroelastic stability, the dynamic characteristics of blades related to pitch angle and the amplitude of lag motion for the rotor equipped with SMA damper were examined. The performance of SMA damper on ground resonance instability are presented through the frequencies and modal damping with respect to rotating speed.

Key Word : Passive damping, shape memory alloy, helicopter rotor blade, stability augmentation

Introduction

Since the hingeless and the bearingless main rotors of helicopter are usually as a soft-inplane rotor, it is susceptible to aeroelastic and aeromechanical instabilities. These dynamic instabilities are generally caused by coupling of blade regressing lag mode and fuselage motions. The instabilities appear when the rotating lag frequency is less than 1/rev, as is typical for articulated and soft-inplane hingeless and bearingless rotors. With the advent of soft in-plane hingeless rotors by the advantage of mechanical simplicity, the ground resonance became one of the major concerns for the hingeless and bearingless rotors. To alleviate these instabilities, most rotors of helicopter need to be equipped with lag dampers[1].

In this paper, the possibility that SMA damper with hysteresis characteristics can be used as a helicopter damper is studied. The most well-known form of transformation behavior exploited in SMAs is thermally induced shape change, often called the shape memory effect. A material component may be strained at low temperatures, and when heated, it reverses this strain and remembers its prestrained shape. In contrast, superelastic effect, known also as pseudoelastic, describes material strains that are recovered isothermally to yield mechanical shape memory

* Research assistant, currently works for Korea Aerospace Research Institute
** Research assistant, currently works for LG CNS
*** Professor, Director of Flight Vehicle Research Center, corresponding author
E-mail : sjkim@snu.ac.kr Tel : 02-880-7388 Fax : 02-887-2662

behavior. If the austenitic phase is strained by an applied load, a martensitic phase is induced by stress, and the twinning process occurs as if the material had been cooled to its martensitic temperature. When the applied load is removed, the material inherently prefers the austenitic phase at the operating temperature, and its strain is instantly recovered[2]. The stress-strain curve indicates a difference in stress levels during loading and unloading, that is known as superelastic stress-strain hysteresis[3,4]. A superelastic specimen exhibits normal elastic behavior until a critical stress is reached. Under further stressing, the specimen elongates substantially, as if it were plastically deformed. However when the stress is removed, the specimen contracts to its original dimensions, and the apparent plastic strain is recovered.

Yet not much research has been conducted for the superelastic damping capacities of SMA under dynamic conditions[5,6]. Some of researchers have examined the effects of frequency of harmonic excitation on the damping characteristics. Piedboeuf and Gauvin [7]studied the effects of frequency and strain amplitude as well as temperature on the damping behavior of superelastic NiTi shape memory alloy wires. They showed that an increase in strain amplitude produces both an increase in dissipated energy and the loss factor. As the frequency continues to increase, there is a pronounced decrease in these two parameters and a sharp decrease of the hysteresis was observed. Gandhi [8,9] investigated energy dissipation of SMAs under a cyclic loading up to 10 Hz. The energy dissipated per unit volume initially decreases rapidly up to 1-2 Hz, and then appears to approach a stable level by 10 Hz. The relatively large energy dissipation potential of shape memory alloy, demonstrated in that study, suggests that it is an attractive potential candidate material for vibration damping[10,11]. Despite a reduction in available damping with increasing frequency, it was noted that the energy dissipated per unit volume by SMAs was still substantially larger than that obtained by using typical elastomeric damping materials.

In this study, shape memory alloy damper with characteristics of pseudoelastic hysteresis for helicopter rotor blades are investigated. An experimental tests of the effects of pre-strain and cyclic strain amplitude as well as frequency on the damping behavior of pseudoelastic shape memory alloy wires are performed. The effects of the shape memory alloy damper on aeroelastic and ground resonance stability of helicopter are studied. In aeroelastic stability, the dynamic characteristics of blades related to pitch angle and the amplitude of lag motion for the rotor equipped with SMA damper were examined. The performance of SMA damper on ground resonance instability are presented through the frequencies and modal damping with respect to rotating speed.

Experiment tests for SMAs

Experimental apparatus and procedure

The material was a NiTi SMA wire with a diameter of 0.5 mm. The specimen used in the tests consists of ten wires bundle. The initial length of the wire between both grips of a testing machine was 70 mm. All of the tests were conducted at a room temperature. Axial force and displacement were measured by a load cell and LVDT, respectively. The stress-strain tests were conducted by subjecting the wire to an initial static displacement and then harmonically oscillating around this offset strain value with a specified cyclic strain amplitude and frequency. The sinusoidal deformation $\varepsilon = \varepsilon_{offset} + \varepsilon_{amplitude} \sin(2\pi ft)$ in a displacement controlled mode is generated. The parameters in this study were the frequency of excitation, offset strain amplitude, and cyclic strain amplitude. The values of these parameters are shown in Table 1. The wires are cycled 100 times to reach a steady state condition under maximum strain at room temperature.

Table 1. Parameters used in the tests

Frequency (Hz), f	0.01, 0.1, 1, 2, 4, 6, 8
Offset strain (%), ε_{offset}	2, 3, 4, 5, 6, 7
Cyclic strain (%), $\varepsilon_{amplitude}$	1, 2, 3, 4

Test results

Influence of offset strain amplitude

To illustrate the effect of strain offset amplitude, the stress-strain curves obtained for the various offset strain amplitude ε_{offset} at a certain frequency and cyclic strain amplitude are shown in Figures 1a, 1b and 1c. Figure 1a shows stress-strain curves for different pre strains of ε_{offset} = 2~7% at a frequency of 0.01Hz with a cyclic strain amplitude of 1%. As shown in Figure 1a, the hysteresis loop area is maximum at the smallest pre strain offset and decreases with increase of offset amplitude. The effect of the offset strain amplitude on hysteresis loop at the cyclic strain amplitude of 2% is plotted in Figure 1b. The martensitic transformation becomes clear and the area of hysteresis loop increases with decreasing offset strain amplitude. As shown in Figure 1b, the forward transformation stress and the reverse transformation stress decrease with the increase in ε_{offset}. The strain-stress curves obtained in the test of SMA wires for the case that exciting frequency is 2Hz at 1% cyclic stain amplitude are shown for the different offset strain amplitude in Figure 1c. As seen in Figure 1a and 1c, the martensite start stress and the austenite start stress increase with increasing frequency. Thus the area of hysteresis loop decreases as the frequency increase. Figure 2 shows the amount of energy dissipated per unit volume with respect to offset strain amplitudes and exciting frequencies. In Figure 2, results are presented from 0.01 Hz to 6 Hz of frequencies up to offset strain amplitude of 6%. It is seen that there is a decrease in the energy dissipation as the offset strain amplitude increase.

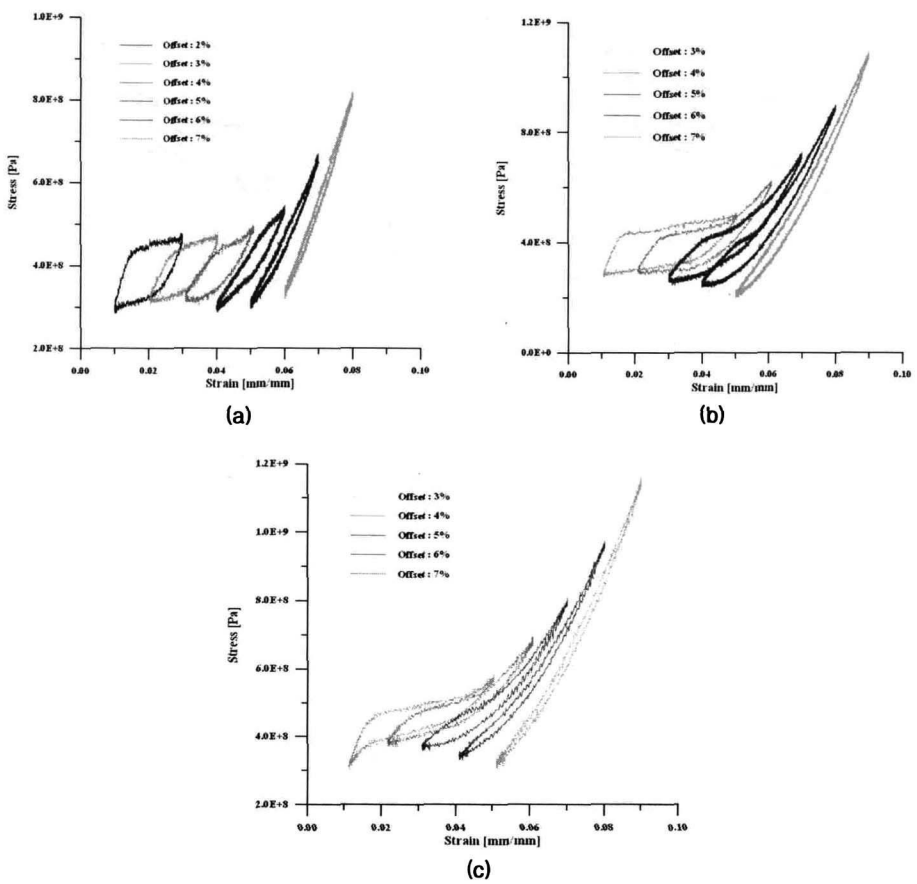

(a) 0.01 Hz and 1% $\varepsilon_{amplitude}$, (b) 0.01 Hz and 2% $\varepsilon_{amplitude}$, (c) 2 Hz and 1% $\varepsilon_{amplitude}$

Fig. 1. Stress-strain curves varying the offset strain amplitude

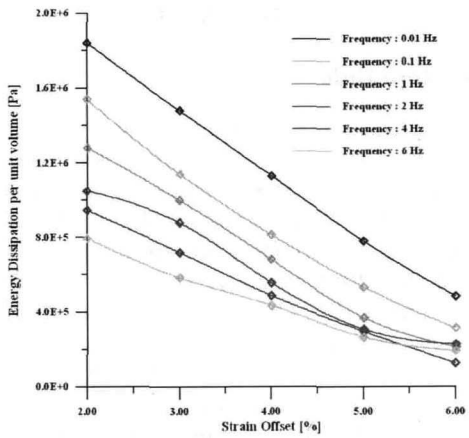

Fig. 2. Energy dissipation with respect to offset strain amplitude (1% $\varepsilon_{amplitude}$)

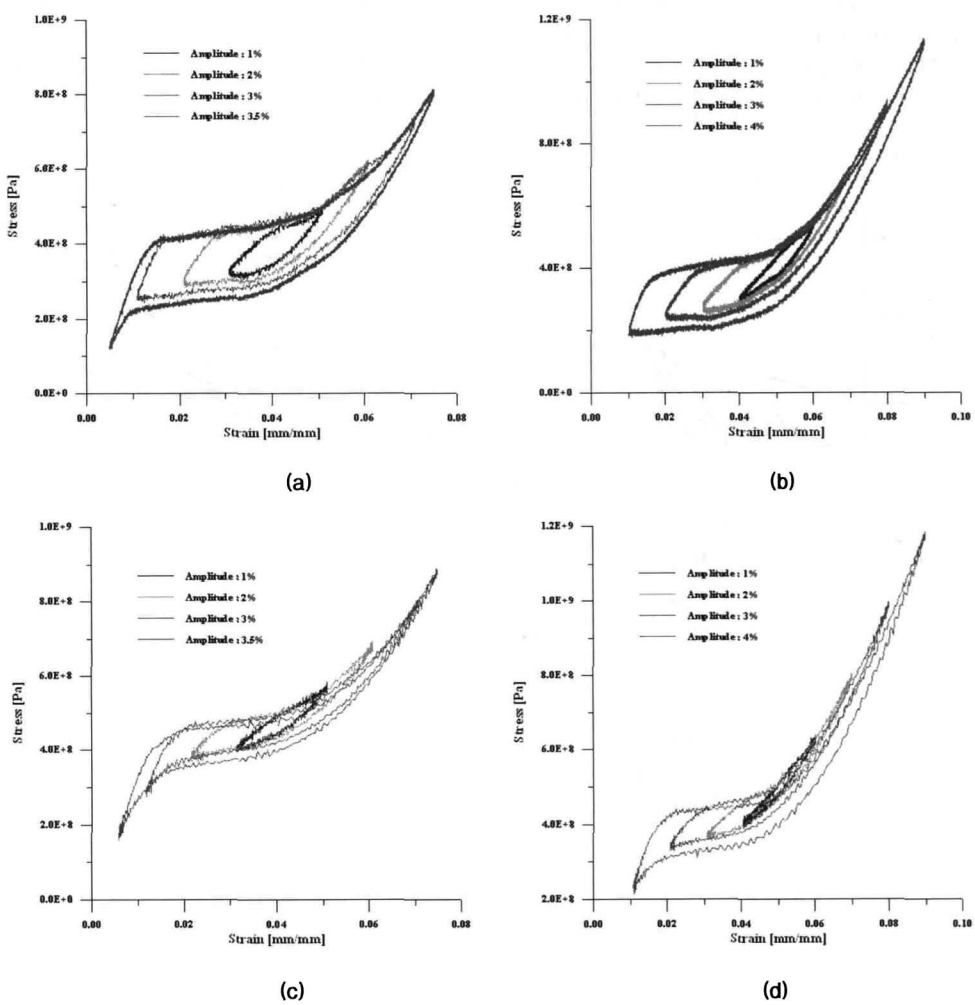

(a) 0.01 Hz and 1% ε_{offset} , (b) 0.01 Hz and 5% ε_{offset} , (c) 2Hz and 4% ε_{offset}, (d) 2 Hz and 5% ε_{offse}

Fig. 3. Stress-strain curves varying the cyclic strain amplitude

Influence of cyclic strain amplitude

Figures 3a-d depict stress-strain curves of SMA wires varying cyclic strain amplitude of $\varepsilon_{amplitude}$ = 1~4% at various frequencies and offset strain amplitude. The effect of the cyclic strain amplitude on the stress-strain curve at 0.01 Hz and 1%ε_{offset} is shown in Figure 3a. The interior hysteresis loops appear for varying cyclic strain amplitude in the Figure 3a. As seen in Figures 3a-d, the forward transformation paths in all interior loops are same, but the reverse transformation paths do not remain the same for the loops. The austenite transformation stresses decrease as the cyclic strain amplitude increases. The stress-strain curves at the frequency of 0.01Hz and offset strain amplitude of 5% ε_{offset} are shown in Figure 3b. Figures 3c and 3d shows the stress-strain curves at the frequency of 2Hz. The hysteresis area decreases with increase of frequency under same cyclic strain amplitude. Figure 4 represents energy dissipation of the SMA wire as a function of cyclic strain amplitude, for various frequencies up to 8 Hz. As expected, increasing the strain amplitude causes the amount of energy dissipation to increase.

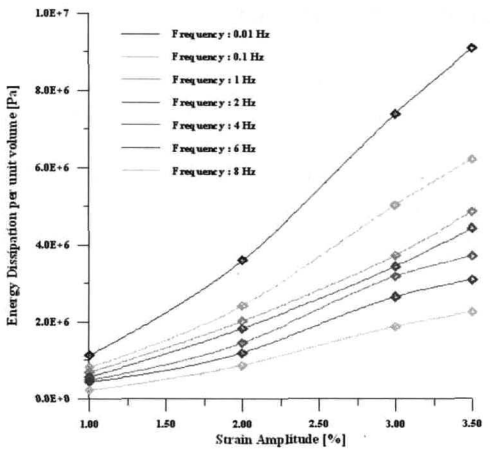

Fig. 4. Energy dissipation with respect to cyclic strain amplitude (4% ε_{offset})

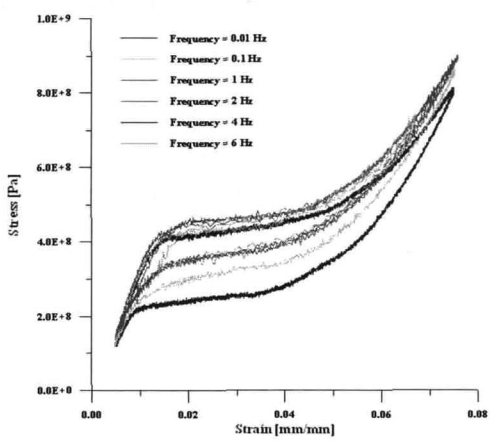

Fig. 5. Stress-strain curves varying the exciting frequency (3.5% $\varepsilon_{amplitude}$ and 4% ε_{offset})

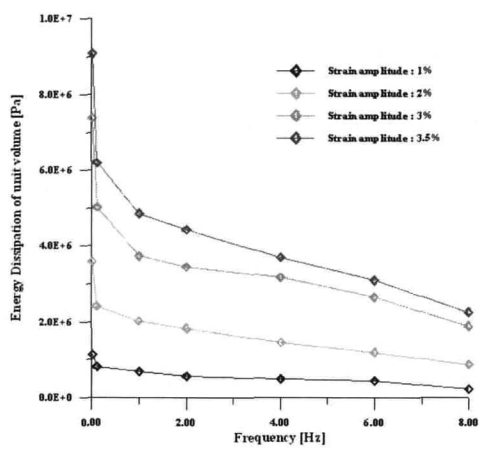

(a)

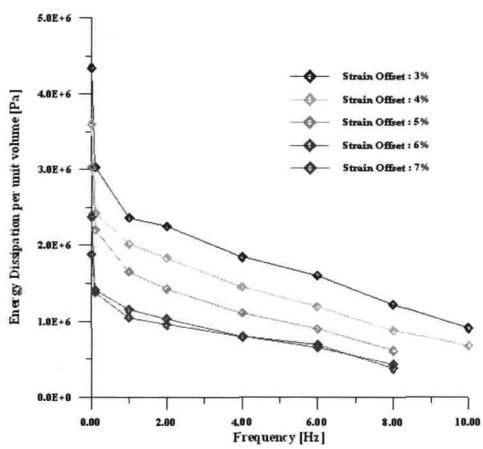

(b)

Fig. 6. Energy dissipation with respect to frequency (a) 4% ε_{offset} , (b) 2% $\varepsilon_{amplitude}$

Influence of exciting frequencies

Figure 5 shows the pseudoelastic hysteresis loops at frequencies from 0.01Hz to 6Hz, for 4% ε_{offset} and 3.5% $\varepsilon_{amplitude}$. It can be easily seen from this figure that while the forward transformation path remains relatively unchanged, the reverse transformation path changes significantly with the low frequencies of 0.01Hz and 0.1Hz. Above 1Hz, the reverse transformation path also seems to be unchanged. From the Figure 5 it is clear that the area of the hysteresis loop decreases as the frequency increases. The initial increase in energy dissipated per cycle at very low frequencies is caused by the decrease in the reverse transformation stress which results in an increase in the hysteresis loop area. Figures 6a and 6b show the energy dissipation per unit volume as a function of frequency. The results in Figure 6a and 6b are presented for the cases of 4% ε_{offset} and 2% $\varepsilon_{amplitude}$, respectively. From these figures, a rapid decrease in the energy dissipation is seen at low frequencies. Thereafter, further decreases in energy dissipation are relative smaller.

Application of helicopter rotor blades

Shape memory alloy damper with characteristics of pseudoelastic hysteresis is applied to helicopter rotor blades to enhance stability. The effects of the shape memory alloy damper on aeroelastic and ground resonance stability of helicopter are studied. In aeroelastic stability, the dynamic characteristics of blades related to pitch angle and the amplitude of lag motion for the rotor equipped with SMA damper are examined. The performance of SMA damper on ground resonance instability are presented through the frequencies and modal damping with respect to rotating speed.

SMA damper force

The SMA wires can be used as damper to enhance stability since SMAs have superelastic effect. Figure 7 shows SMA wire damper instead of an elastomer damper commonly used to helicopter rotor blades. SMA damper consisting of several wires bundle has an influence on the rotor dynamics due to changing stiffness and damping. The steady lagging motion of blade causes the wires to strain initially and cyclic loading is applied to SMA wires when blade lag motion vibrates. Thus the vibration can be damped due to SMA pseudoelastic characteristics. In Figure 7, h is the distance from the lag hinge to SMA damper and l is the initial wires length when no loading is applied.

The pseudoelastic SMAs materials can be highly nonlinear. While their dynamic characteristics are dependent on many factors such as offset strain amplitude, frequency, and temperature, the most significant variation occurs as a function of dynamic strain amplitude. In the application of SMA damper, it is important to know the effect of changes in the damper characteristics on the stability. To determine this, the complex modulus approach was used. The real part of complex modulus, which is in phase with the displacement, represents the stiffness modulus and the imaginary part of it, E'', which is 90° out of phase with the displacement, represents the damping modulus. The loss factor(η) is defined as the ratio of the damping modulus to the stiffness modulus. From the complex modulus method, the stiffness modulus and loss factor of the SMA wires was measured as a function of cyclic strain amplitude. Figure 8 shows measured stiffness and loss factor of SMA wires as a function of cyclic strain amplitude at 2Hz and 4% ε_{offset} . From the second order a least-squares polynomial curve fit to the measured value, the stiffness modulus and loss factor with respect to strain amplitude are expressed as follows:

$$E' = (17.5535 - 860.878\varepsilon + 17129.6\varepsilon^2)[GPa] \tag{1}$$

$$\eta = (0.308 + 12.505\varepsilon - 433.991\varepsilon^2) \tag{2}$$

Thus, damper moment about lag hinge can be written as follows:

$$M_D = \frac{Ah^2}{l}\left\{E'\varsigma + \frac{E''}{\omega}\dot{\varsigma} + (E_0 - E')\varsigma_0\right\} \tag{3}$$

where A, ω, and ζ is the total section area of SMA wires bundle, the lag natural frequency, and lag angle. The E_0 is the stiffness at the pre-strain due to steady lagging. The first term represents stiffness of damper, the second term is the equivalent viscous damping from the damper, and the others is related to offset strain amplitude.

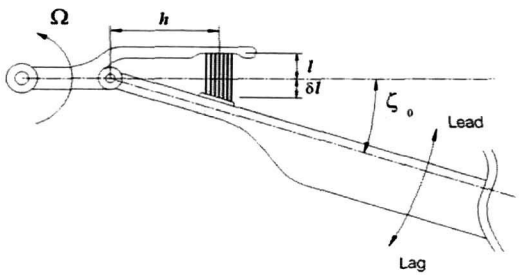

Fig. 7. Helicopter rotor blade with SMA wire damper

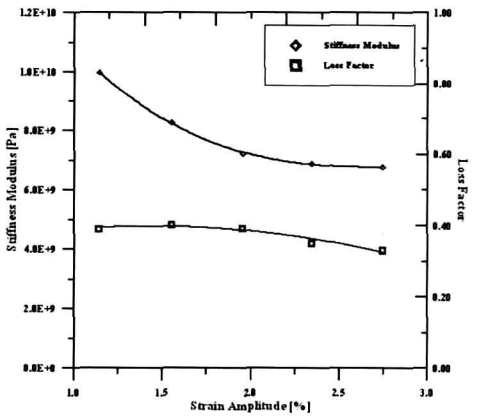

Fig. 8. Stiffness modulus and loss factor of SMA wires as a function of cyclic strain amplitude at 2Hz and 4% pre-strain

Aeroelastic stability in hover

The fundamental stability characteristics of helicopter rotor blades can be studied by retaining only the flap and lead-lag degrees of freedom of a single blade. The blade is assumed to be rigid and it has a hinge offset at a distance e from the rotating axis. This simple configuration represents an articulated blade with lag hinge and flap hinge and can be an approximate representation for a hingeless blade with a possible leaf spring at the hinge. The aerodynamic loading can be expressed including the effects of flap and lag velocities from simple strip theory. Considering moment equilibriums due to inertial forces, aerodynamic forces, elastic force, and damper force, the flap-lag perturbation equation are obtained as follows:

$$\begin{bmatrix}1 & 0\\ 0 & 1\end{bmatrix}\begin{Bmatrix}\ddot{\beta}\\ \ddot{\varsigma}\end{Bmatrix} + \begin{bmatrix}\frac{\gamma}{8}\left(1+\frac{C_{d0}}{a}\right) & -\frac{\gamma}{8}\left\{2\theta - \left(1+\frac{C_{d0}}{a}\right)A\right\} + 2\beta_0\\ \frac{\gamma}{8}(\theta - 2A) - 2\beta_0 & \frac{\gamma}{8}\left(2\frac{C_{d0}}{a} + A\theta\right) + \Lambda^2\end{bmatrix}\begin{Bmatrix}\dot{\beta}\\ \dot{\varsigma}\end{Bmatrix} + \begin{bmatrix}\nu_\beta^2 & 0\\ 0 & \nu_\varsigma^2\end{bmatrix}\begin{Bmatrix}\beta\\ \varsigma\end{Bmatrix} = \begin{Bmatrix}\frac{\gamma}{8}\Delta\vartheta\\ -\frac{\gamma}{8}A\end{Bmatrix} \tag{4}$$

where, $\Lambda^2 = \frac{K_d''}{I\nu_\varsigma\Omega^2} = \frac{\eta}{\nu_\varsigma}\frac{w_{\rho 0}^2}{\Omega^2}\overline{K}$ is damper properties and lag frequency ν_ζ is given by:

$$\nu_\varsigma^2 = \frac{e\int_e^R m(\gamma - e)dr}{I_\xi} + \frac{w_{\rho 0}^2}{\Omega^2}\left(1 + \frac{K_d'}{K_\xi}\right) \tag{5}$$

Where, A, γ , θ , ν_β is inflow parameter defined in reference 15, Lock number, and pitch angle, and flap frequency, respectively. The two terms in the damper moment contribute directly to the lag equation of motion as equivalent viscous damping and as an addition to the rotation lag frequency.

Figure 9 represents the root loci of flap and lag modes for increasing pitch angle. Flap mode

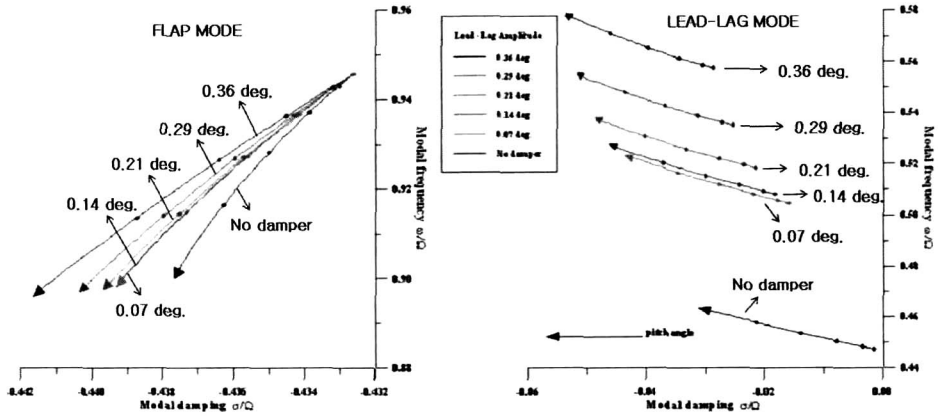

Fig. 9. Locus of roots for increasing pitch angle for flap mode and lag mode

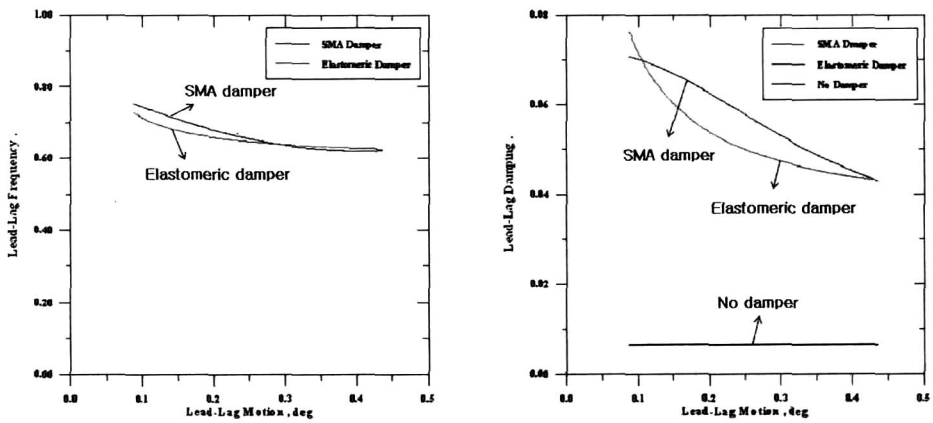

Fig. 10. Comparison between SMA damper and elastomeric damper for lag motion.

is highly damped at entire pitch angles. The damping increases and the frequency decrease with the increase of pitch angle as seen in Figure 9. As the lead-lag motion increases, the damping also increases. In Figure 9, the lag mode is inherently weak in instabilities due to small damping. In lag mode, the damping increases as the pitch angle increases. The lag mode frequency increases as lag motion increases. This tendency is not good in designing blades. It is difficult to design the rotor if the frequency is changed under a certain operation environment since some instabilities occur. However, this phenomenon may occur at the elastomeric lag damper conventionally used in helicopter. Thus it is not big problem. With SMA damper, the lag mode damping increases significantly with the increase of pitch angle as shown in Figure 9. In Figure 10, comparison between SMA damper and elastomeric damper was made for lag mode frequency and damping. The variation of frequency for SMA damper is almost similar to that for elastomeric damper. Considering the amount of damping, the difference between both damper is small or the case with SMA damper is slightly higher than that with elastomeric damper.

Ground resonance stability

In order to clearly identify the effects of the damper on ground resonance stability of helicopter, a simplified mathematical model of the helicopter is considered for the numerical studies in this paper. The rigid fuselage undergoes x- and y-hub motion, and the rigid blades

undergo lag motions. For ground resonance studies, the effects of aerodynamics, which are known to be small, are neglected. Each blade has a rotating spring k_ζ and SMA wire damper which act about the lag hinge. The effect of the SMA damper on ground resonance stability is investigated using the classical four-degree-of-freedom model of Coleman and Feingold.

Figures 11a and 11b show the Coleman diagram for a soft-inplane hingeless rotor helicopter without damper and with SMA damper, respectively. The Coleman diagram consists of a plot of frequencies as a function of rotational speed. The frequencies corresponding to different modes in the fixed frame are obtained from eigen-solutions. The data in the Table 2 is used for calculations. The nondimensional lag frequency at the operating speed is v_ζ = 0.62/rev without damper. These diagrams show that the coalescence of the regressive lag mode with the fuselage modes is weaker due to the presence of the SMA damper. Figures 12a and 12b show the modal damping of the rotor with SMA damper when there are no fuselage support damping and moderate support damping, respectively. In the case of no support damping as shown in Figure 12a, two instability bands exist. The instability remains in the crossover regions of the pitch and roll mode of fuselage without damper. This shows that a large damping is required to stabilize this instability. In the case with SMA damper, the damping with hysteresis characteristics has a weak instability effect on the blades as shown in Figure 12a. The Figure 12b for including moderate fuselage support damping shows that the instabilities for the case with damper disappear over the entire rotating speed range, while the instabilities for no damper still remains.

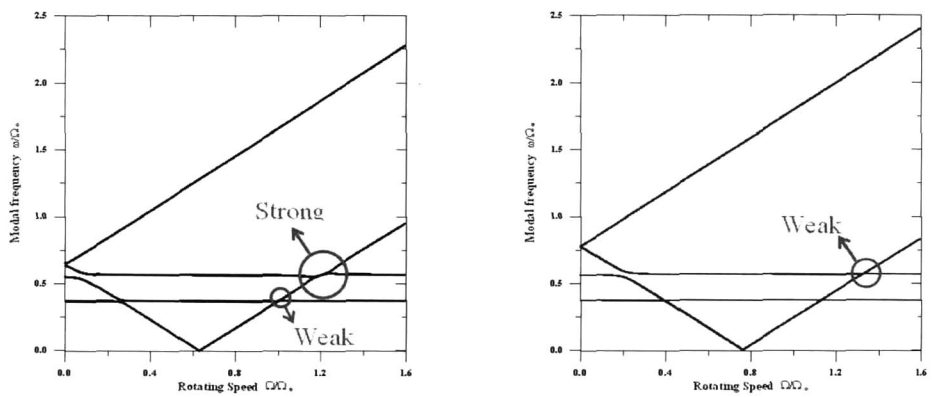

Fig. 11. Coleman diagram for ground resonance. (a) no damper, (b) SMA damper

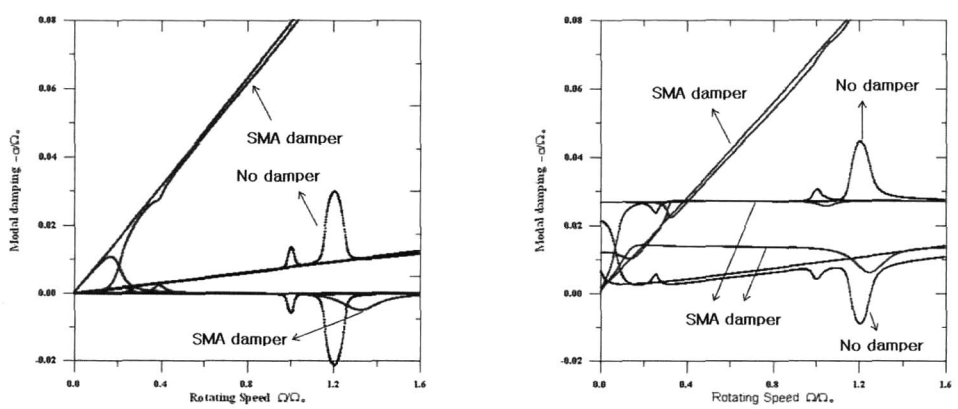

(a) without support damping , (b) with inclusion of moderate support damping.

Fig. 12. Modal damping for ground resonance

Table 2. Rotor parameters used in the simulation

No. of blades	4	Hub spring, K_y	1240481.8 N/m
Blade mass	73.89 kg	Fuselage support frequency w_x	12.2089 rad/s
Blade mass moment S_ζ^*	1.5	Fuselage support frequency w_y	18.6188 rad/s
Lag hinge offset, e	0.093	Lag inertia, I_ζ	691.47 kgm^2
Blade lag frequency	0.62/rev	Lag stiffness, K_ζ	1197.5 Nm
Hub mass, M_x	8026.6 kg	Rotor speed	314 RPM
Hub mass, M_y	3283.6 kg	Support damping ratio, C_x	0.073
Hub spring, K_x	1240481.8 N/m	Support damping ratio, C_y	0.0482

Concluding remarks

In this work, the characteristics of pseudoelastic effects of shape memory alloys are examined to augment the stability of helicopter rotors. An experimental study of the effects of pre-strain and cyclic strain amplitude as well as frequency on the damping behavior of pseudoelastic NiTi shape memory alloy wires is undertaken. As the frequency and the offset strain increase, the energy dissipated by the wires decrease. However, the amount of energy dissipation also increases with increase of the cyclic strain amplitude. The effects of SMA damper on the aeroelastic stability and the ground resonance instability of a helicopter rotor were investigated. From the stabilities analysis, the SMA damper has a strong stabilizing effect on the inherently weakly damped lag mode of the rotor blades.

References

1. Ormiston Robert A., 1983,"Investigations of Hingeless Rotor Stability", *Vertica*, Vol. 7, No. 2, pp. 143-181.

2. Mel Schwartz, *ENCYCLOPEDIA OF SMART MATERIALS, Vol. 2*, John Wiley and Sons, Inc, New York, pp.921-980, 2002.

3. Tanaka, K., 1986."A Thermomechanical Sketch of Shape Memory Effect: One-dimensional Tensile Behavior", *Res. Mechanica*, Vol. 18 : 251-263.

4. Tanaka, K., 1990."A phenomenological description on thermomechanical behavior of shape memory alloys," *Journal of Pressure Vessel Technology*, Vol. 112 : 158-163.

5. Lin, P.H., Tobushi, H., Tanaka, K., Hattori, T., and Makita, M., 1994."Pseudoelastic Behavior of TiNi Shape Memory Alloy Subjected to Strain Variations", *Journal of Intelligent Material Systems and Structures*, Vol. 5 : 694-701.

6. Naito, H., Matsuzaki, Y., Funami, K., andIkeda, T., 2001."Frequency Characteristics of Pseudoelasticity of Shape Memory Alloys", *42ndAIAA/ASME/ASCE/AHS/ASC Structures, Structural Dynamics, and Materials Conference and Exhibit*, Seattle, WA, AIAA-2001-1355.

7. Piedboeuf, M.C., Gauvin, R., and Thomas, M., 1998."Damping behavior of shape memory alloys: strain amplitude, frequency and temperature effects", *Journal of Sound and Vibration*, Vol. 214 : 885-901.

8. Malovrh, B., and Gandhi, F., 2001."Mechanism-Based Phenomenological Medels for the Pseudoelastic Hysteresis Behavior of Shape Memory Alloys", *Journal of Intelligent Material Systems and Structures*, Vol. 12, No. 1.

9. Gandhi, F., and Wolons, D., 1999."Characterization of the Pseudoelastic Damping Behavior of Shape Memory Alloy Wires using Complex Modulus", *Smart Materials and Structures*, Vol. 8 : 49-56.

10. Muller, I., and Xu, H., 1991."On the pseudo-elastic hysteresis", *Acta Metallic Materials*, or Acta metallurgica et materialia Vol. 39 : 263-271.

11. Thompson, P., Balas, G.J., and Leo, P.H., 1995."The Use of Shape Memory Alloys for Passive Structural Damping", *Smart Materials and Structures*, Vol. 4 : 36-41.

12. Kim, J.S., and Yun, C.Y., 2001."Performance Comparison between Piezoelectric and Elastomeric Lag Dampers on Ground Resonance Stability of Helicopter", *Journal of Intelligent Material Systems and Structures*, Vol. 12, No. 4. : 215-222.

13. Coleman, R. P. and Feingold, A. M., 1956, "Theory of Self-Excited Mechanical Oscillation of Helicopter Rotors with Hinged Blades", NACA TR-1351.

14. Hammond, C. E., 1974, "An application of Floquet theory to the prediction of mechanical instability", *Journal of the American Helicopter Society*, Vol.19, No.4, pp. 14-23.

15. Ormiston, R. A. and Hodges, D. H., 1972, "Linear Flap-Lag Dynamics of Hingeless Helicopter Rotor Blades in Hover", *Journal of the American Helicopter Society*, Vol.17, No.2.